Fusion and quasifission studies in reactions forming Rn via evaporation residue measurements

A. Shamlath,[1] E. Prasad,[1,*] N. Madhavan,[2] P. V. Laveen,[1] J. Gehlot,[2] A. K. Nasirov,[3,†] G. Giardina,[4] G. Mandaglio,[5,‡] S. Nath,[2] Tathagata Banerjee,[2] A. M. Vinodkumar,[6] M. Shareef,[1] A. Jhingan,[2] T. Varughese,[2] DVGRKS Kumar,[7] P. Sandya Devi,[7] Khushboo,[8] P. Jisha,[6] Neeraj Kumar,[8] M. M. Hosamani,[9] and S. Kailas[10]

[1]*Department of Physics, School of Physical Sciences, Central University of Kerala, Kasaragod 671314, India*
[2]*Inter University Accelerator Centre, Aruna Asaf Ali Marg, New Delhi 110067, India*
[3]*BLTP, Joint Institute for Nuclear Research, Joliot-Curie 6, Dubna 141980, Russia*
[4]*Dipartimento MIFT dell' Università di Messina, Salita Sperone 31, 98166 Messina, Italy*
[5]*Dipartimento ChiBioFarAm dell' Università di Messina, Salita Sperone 31, 98166 Messina, Italy*
[6]*Department of Physics, University of Calicut, Calicut 673635, India*
[7]*Department of Nuclear Physics, Andhra University, Visakhapatnam 530003, India*
[8]*Department of Physics and Astrophysics, University of Delhi, New Delhi 110007, India*
[9]*Department of Physics, Karnatak University, Dharwad 580003, India*
[10]*UM-DAE Centre for Excellence in Basic Sciences, University of Mumbai, Mumbai 400098, India*

(Received 19 November 2016; revised manuscript received 21 January 2017; published 17 March 2017)

Background: Formation of the compound nucleus (CN) is highly suppressed by quasifission in heavy-ion collisions involving massive nuclei. Though considerable progress has been made in the understanding of fusion-fission and quasifission, the exact dependence of fusion probability on various entrance channel variables is not completely clear, which is very important for the synthesis of new heavy and superheavy elements.
Purpose: To study the interplay between fusion and quasifission in reactions forming CN in the boundary region where the fusion probability starts to deviate from unity.
Methods: Fusion evaporation residue cross sections were measured for the ^{28,30}Si + ^{180}Hf reactions using the Hybrid Recoil Mass Analyser at IUAC, New Delhi. Experimental data were compared with data from other reactions forming the same CN or isotopes of the CN. Theoretical calculations were performed using the dinuclear system and statistical models.
Results: Reduced evaporation residue cross sections were observed for the reactions studied compared with the asymmetric reaction forming the same CN, indicating fusion suppression in more symmetric systems. The observations are consistent with fission fragment measurements performed in the same or similar systems. Larger ER cross sections are observed with increase in mass in the isotopic chain of the CN.
Conclusions: Fusion probability varies significantly with the entrance channels in reactions forming the same CN. While complete fusion occurs for the ^{16}O + ^{194}Pt reaction, the fusion probability drops to approximately 60–70% for the ^{30}Si + ^{180}Hf and less than 20% for the ^{50}Ti + ^{160}Gd reactions, respectively, forming the same CN at similar excitation energies.

DOI: 10.1103/PhysRevC.95.034610

I. INTRODUCTION

Remarkable progress has been achieved in recent years in the synthesis of new heavy and superheavy elements (SHE) [1–3] using heavy-ion fusion reactions. Elements up to $Z = 118$ have been successfully synthesized in the laboratory. The production cross sections of the superheavy evaporation residues (ER) in SHE synthesis are very low, often of the order of picobarns or less [1,3]. Conceptually, the process of formation of an ER in heavy-ion fusion reaction is considered to be a sequence of three stages—the capture of the projectile and target inside the potential pocket, formation of a completely equilibrated composite nucleus called CN, and CN survival against fission. It may be noted that the above factorization of ER formation as three steps is only a matter of convenience and they are not independent of each other in reality. However, these steps are distinct enough for a qualitative discussion. The time scales involved in these different stages are also different. Hence, the ER cross section may be treated as the product of capture cross section, CN formation probability, and the probability of survival against fission.

For fusion involving light, very asymmetric systems, overcoming the capture barrier automatically leads to the formation of the CN. For such systems, the contact configuration itself will be inside the unconditional saddle configuration [4,5]. Hence, the fusion probability P_{CN} is always unity for collisions involving such nuclei. For heavier systems, overcoming the capture barrier does not guarantee the formation of the CN as the contact configuration could be outside the unconditional saddle point and the system may reseparate before achieving

*Present address: Department of Nuclear Physics, Australian National University, Canberra ACT, Australia; prasad.e.nair@gmail.com.
†Present address: National University of Uzbekistan, 100174 Tashkent, Uzbekistan.
‡Present address: Instituto Nazionale di Fisica Nucleare, Sezione di Catania, Italy.

the compact shape of the CN. P_{CN} is significantly less than unity in such cases. One of the major noncompound nuclear processes is quasifission [4,6,7], which is partly responsible for the low production cross sections in SHE synthesis. Today, quasifission is known to have strong dependence on entrance channel properties [8–13] and is also sensitive to the structural aspects of nuclei such as static deformation [14–17], shell closure [18,19], and the N/Z of the projectile and target nuclei [18] involved in the reactions.

The competition between fusion and quasifission decides the fusion probability P_{CN}. The quasifission probability increases with the increase in the charge product $Z_P Z_T$, where Z_P and Z_T are the atomic numbers of the projectile and target nuclei, respectively. For this reason, quasifission is the dominant outcome in superheavy element formation reactions, resulting in $P_{CN} \ll 1$. A detailed understanding of fusion and quasifission is thus highly required for the selection of optimum reaction for the SHE synthesis. The onset of quasifission was predicted in nuclear collisions with $Z_P Z_T \geqslant 1600$ [4] earlier. However, a number of measurements have reported the onset of quasifission for systems with much lower $Z_P Z_T$ values [8,20,21]. A systematic analysis [22] of ER cross section data for a number of reactions leading to CN in the mass region of 170–220 a.m.u. recently reported approximate boundaries from where the average fusion probabilities deviate from unity. Hence, it will be interesting to explore the interplay between fusion and quasifission in reactions forming nuclei in this boundary region where fusion probability starts to deviate from unity.

In this work, we present the results of ER excitation function measurements for the ^{28,30}Si + ^{180}Hf reactions forming the CN ^{208,210}Rn, respectively. ER cross sections for the reactions ^{28,29}Si + ^{178}Hf populating the CN ^{206,207}Rn are available in literature [23,24]. Hence an extensive study of Si+Hf reactions populating different isotopes of Rn as well as a few other reactions populating the same CN or isotopes of the same CN reported in literature are performed in this paper. The paper is organized in the following sequence: Experimental details, data analysis, and experimental results are described in Secs. II–IV, respectively. The details of theoretical calculations performed are discussed in Sec. V, followed by the discussion of theoretical and experimental results in Sec. VI. In Sec. VII, we summarize our findings and conclude this work.

II. EXPERIMENTAL DETAILS

The ER excitation function measurements were performed using the accelerator facilities at the Inter University Accelerator Centre (IUAC), New Delhi. Pulsed beams of ^{28,30}Si with pulse separation of 2 μs from the 15 UD Pelletron accelerator were further boosted using the superconducting linear accelerator (SC-LINAC) [25,26] to bombard the isotopically enriched ^{180}Hf target of thickness 150 μg/cm^2 on a 40 μg/cm^2 thick carbon backing, with carbon backing facing the beam.

The low-intensity ERs produced in the reactions were separated from the intense beam background using the Hybrid Recoil Mass Analyzer (HYRA) [27,28] operated in gas-filled mode. HYRA is a dual-mode, dual-stage separator with its first stage capable of operating in gas-filled mode in normal kinematics. Due to the velocity and charge state focusing, a gas-filled separator offers better transmission efficiency compared to its vacuum-mode counterparts. Helium gas at an optimized pressure of 0.20 mbar was used in the energy range of present measurements. The magnetic field settings of HYRA magnets were optimized by scanning the field values within a range of ±10% of the calculated values [29] and the transmission through the separator was maximized at each measured energy. A pressure window foil made of carbon with 650 μg/cm^2 thickness was used to separate the beam-line vacuum from the gas-filled region of HYRA.

The measurements were performed at laboratory beam energies of 130.6, 135.0, 143.9, 149.4, 154.9, 164.2, 171.9, and 193.7 MeV for the ^{28}Si + ^{180}Hf reaction and 130.6, 135.2, 139.6, 144.0, 149.5, 156.3, 160.7, 164.3, and 171.8 MeV for the ^{30}Si + ^{180}Hf reaction, respectively. The energies mentioned above for different beams are the average energies in the middle of the target, which were obtained after correcting the energy loss of the beam particles in 650 μg/cm^2 carbon (pressure window foil), 0.2 mbar of He gas (between the window foil and target which is at ∼20 cm away), 40 μg/cm^2 carbon (backing), and 75 μg/cm^2 of ^{180}Hf (half-target thickness). The ERs guided to the focal plane of HYRA were detected using a position-sensitive multiwire proportional counter (MWPC) [30] of active area 15 cm × 5 cm followed by a silicon strip detector of active area 5 cm × 5 cm. The gas detector was operated with isobutane gas of about 2.5 mbar pressure. A large area mylar foil of thickness 0.5 μm was used to separate HYRA electromagentic section and the focal plane detectors. The MWPC detector provided position (X and Y), energy loss (ΔE), and timing signals. A time-of-flight (TOF) spectrum was generated using the timing pulse from the MWPC anode signal as the start and the suitably delayed radio frequency (RF) signal with 2 μs pulse separation as the stop. The ΔE versus TOF spectrum enabled an unambiguous identification of the ERs from other possible scattered particles reaching the focal plane. Figure 1 shows the two-dimensional plot of ΔE versus TOF at 130.6 MeV beam energy for the ^{28}Si + ^{180}Hf reaction.

Two silicon detectors were used inside the target chamber, placed at $\theta = \pm 25^\circ$ to detect the elastically scattered beam

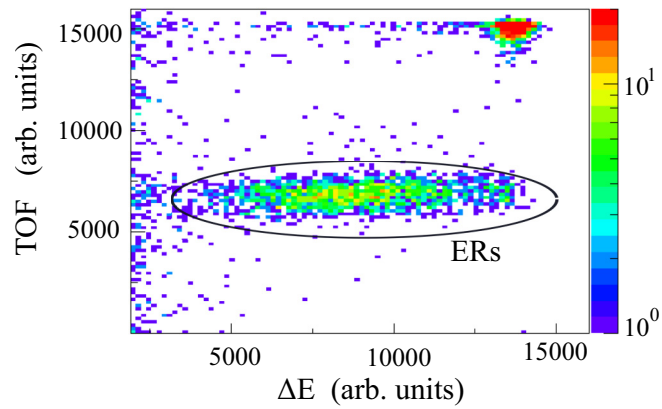

FIG. 1. Two-dimensional plot of ΔE vs TOF for the reaction ^{28}Si + ^{180}Hf at 130.6 MeV energy.

particles for absolute normalization of the ER cross sections. These detectors were also used for positioning the beam at the center of the target throughout the experiment.

III. DATA ANALYSIS

The total ER cross sections ($\sigma_{\rm ER}$) were calculated using the equation

$$\sigma_{\rm ER} = \frac{Y_{\rm ER}}{Y_{\rm mon}}\left(\frac{d\sigma}{d\Omega}\right)_R \Omega_M \frac{1}{\varepsilon_{\rm HYRA}}. \quad (1)$$

Here, $Y_{\rm ER}$ is ER yield at the focal plane, $Y_{\rm mon}$ is the yield of the elastically scattered projectiles registered by the monitor detector, $(\frac{d\sigma}{d\Omega})_R$ is the differential Rutherford scattering cross section in the laboratory frame, Ω_M is the solid angle subtended by the monitor detector, and $\varepsilon_{\rm HYRA}$ is the transmission efficiency of the separator.

The transmission efficiency $\varepsilon_{\rm HYRA}$ is the ratio of the number of ERs reaching the focal plane of HYRA to the total number of ERs emerging out of the target for a given reaction. It a is complex function of several parameters [28,31] such as the entrance-channel mass asymmetry, beam energy, target thickness, the exit channels of interest, angular acceptance of the separator, magnetic field and gas pressure settings of the separator, etc. It also depends on the size of the focal plane detector, particularly when operated in the gas-filled mode.

Different techniques may be used for the experimental measurement of the transmission efficiency [28,31–33] of a recoil mass spectrometer and separator. In this measurement, we used the ^{30}Si + ^{186}W reaction as the calibration reaction to estimate $\varepsilon_{\rm HYRA}$, following the method described in Ref. [28]. The ER cross sections for this reaction are already reported [34]. The total ER cross sections for the calibration reaction were thus measured for different beam energies and the $\varepsilon_{\rm HYRA}$ was calculated for this reaction from the known cross sections using Eq. (1) for each of these measured energies. $\varepsilon_{\rm HYRA}$ obtained for the calibration reaction was used for estimating the same for the ^{28,30}Si + ^{180}Hf reactions in the second step. For this, the ER angular distributions of the ^{28,30}Si + ^{180}Hf reactions were simulated using the TERS code [31] and the normalized distributions were compared with that of the calibration reaction, within the angular acceptance of HYRA. The efficiency obtained for the ^{30}Si + ^{186}W reaction was thus normalized to get the transmission efficiency for the ^{28,30}Si + ^{180}Hf reactions.

It may be mentioned that cross section data are not available for the calibration reaction at 193.7 MeV laboratory energy for a direct calculation of $\varepsilon_{\rm HYRA}$ for the ^{28}Si + ^{180}Hf reaction. Hence, a linear extrapolation has been employed from the calculated $\varepsilon_{\rm HYRA}$ values at the lower energies to estimate the transmission efficiency at 193.7 MeV for the ^{28}Si + ^{180}Hf reaction. This first-order approximation should be valid, as the dependent parameters [31] are not expected to vary significantly with beam energy.

IV. EXPERIMENTAL RESULTS

The total ER cross sections ($\sigma_{\rm ER}$) obtained for the ^{28,30}Si + ^{180}Hf reactions as a function of center-of-mass ($E_{\rm c.m.}$) energy are shown in Fig. 2. The overall errors in the calculated cross sections are <20%, among which $\varepsilon_{\rm HYRA}$ contributes the maximum. The measured ER excitation function shows a decreasing trend at higher beam energies for the ^{30}Si + ^{180}Hf reaction. This might be due to the increased fission competition at larger angular momenta, for which fission barrier falls rapidly, favoring fission decay over particle evaporation. Even though the ^{28}Si + ^{180}Hf reaction also show a similar trend, the cross section at the highest energy (with $E^* = 106$ MeV, see Table I) deviates from the expected trend. This will be discussed in detail in Sec. VI. D. In addition, the experimental cross sections are observed to be larger for the reaction populating the heavier isotope of radon. Measured total ER cross sections for the two reactions studied at different center-of-mass energies are shown in Table I. The corresponding CN excitation energies are also shown.

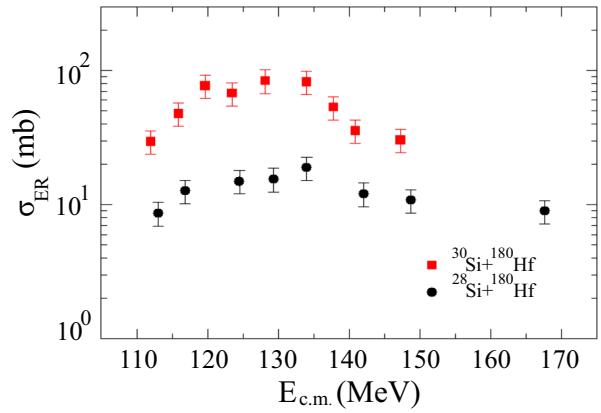

FIG. 2. The experimental ER cross sections for the ^{28,30}Si + ^{180}Hf reactions as a function of center-of-mass energy.

TABLE I. Measured total ER cross sections at different center-of-mass energies for the two reactions studied in this work. Corresponding CN excitation energy E^* is also shown.

Reaction	$E_{\rm c.m.}$ (MeV)	E^* (MeV)	$\sigma_{\rm ER}$ (mb)
	113.0	51.4	8.6 ± 1.7
	116.9	55.2	12.6 ± 2.5
	124.5	62.9	15.0 ± 3.0
^{28}Si + ^{180}Hf	129.3	67.7	15.6 ± 3.1
	134.0	72.4	18.9 ± 3.8
	142.1	80.5	12.1 ± 2.4
	148.7	87.1	10.8 ± 2.2
	167.6	106.0	8.9 ± 1.8
	112.0	47.4	29.6 ± 5.9
	115.9	51.2	47.9 ± 9.6
	119.7	55.0	77.1 ± 15.4
	123.4	58.8	67.9 ± 13.6
^{30}Si + ^{180}Hf	128.1	63.5	84.0 ± 16.8
	134.0	69.4	82.4 ± 16.5
	137.8	73.2	53.4 ± 10.7
	140.9	76.2	35.7 ± 7.2
	147.3	82.6	30.5 ± 6.1

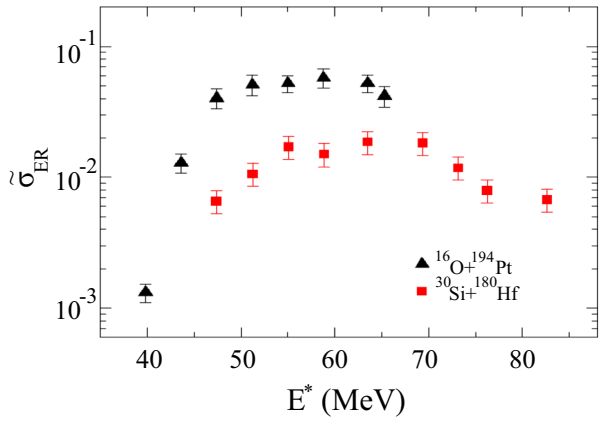

FIG. 3. The reduced ER cross sections for the $^{16}O+^{194}Pt$ and $^{30}Si+^{180}Hf$ reactions populating the CN ^{210}Rn as a function of CN excitation energy.

In Fig. 3, we compare the reduced ER cross sections ($\tilde{\sigma}_{ER}$) for the $^{30}Si+^{180}Hf$ reaction with that of the $^{16}O+^{194}Pt$ reaction populating the same CN [28] at similar excitation energies. The absolute cross sections were converted to reduced cross sections by dividing σ_{ER} by πR_B^2, where R_B is the barrier radius, obtained by using the Akyuz-Winther [35] potential parameters in CCFULL [36]. It may be observed that at similar E^* values the reduced cross sections are larger for the $^{16}O+^{194}Pt$ compared with those for the $^{30}Si+^{180}Hf$ reaction.

The reduction in ER cross sections for the less mass-asymmetric reaction $^{30}Si+^{180}Hf$ could be either due to an increased fission probability or the suppression of fusion due to the onset of quasifission in this reaction. A previous study of fission fragment mass distributions [21] for the same reactions showed larger fission fragment mass widths [21] for the $^{30}Si+^{180}Hf$ reaction at similar E^* values, which could not be explained by theoretical models [37–39] that assume complete fusion. Current observations are also supported by the fission fragment angular distribution studies for a number of reactions populating isotopes of radon or nearby nuclei [40], at energies close to the Coulomb barrier. The reduction in ER cross sections and larger fission fragment mass widths in the $^{30}Si+^{180}Hf$ reaction hence clearly demonstrate the presence of quasifission in this reaction. Such observations for the morethe symmetric reactions compared with asymmetric reaction were previously reported in different reactions populating the CN ^{216}Rn [8,34] and ^{220}Th [41].

V. THEORETICAL CALCULATIONS

The decay of a CN formed in heavy-ion reactions can be well described by statistical models. In statistical model theories, all open channels on the average are equally likely to be populated, when a statistical equilibrium is achieved. Most of the available statistical models assume that the system after capture undergoes the formation of the CN and decay subsequently via all energetically possible decay modes such as particle evaporation, γ decay, and fission. As the $^{30}Si+^{180}Hf$ reaction showed signatures of nonequilibrium processes in the experimental observables such as ER cross sections and fission fragment mass distributions, statistical models could be used to simulate the decay channels only if the P_{CN} values are precisely known. Even though different empirical parametrizations [42–44] exist in literature for estimating the P_{CN}, experimental data show significant differences in many cases [45]. We, in this work, used the dinuclear system model (DNS) to first generate the angular momentum distributions for the CN formation and these distributions were used for the ER cross section calculations at a given value of E^* and angular momentum, ℓ, using an advanced statistical model [46].

TABLE II. Deformation parameters of the ground state and the first excited 2^+ and 3^- states of different nuclei considered in this work.

Nucleus	β_2	β_3	β_2^+ [53]	β_3^- [54]
^{16}O	0.021	0.0	0.364	0.37
^{28}Si	−0.478	0.0	0.407	0.240
^{30}Si	0.0	0.0	0.315	0.275
^{50}Ti	0.0	−0.020	0.166	0.170
^{160}Gd	0.28	0.0	0.353	0.064
^{180}Hf	0.273	0.0	0.274	0.058
^{194}Pt	−0.148	0.0	0.143	0.070

A. DNS model approach

The formation of ER in heavy-ion collision depends on the probabilities of capture, fusion, and survival of the fused system against fission. The probability of fusion and quasifission are highly influenced by the motion of the system, after capture, over the multidimensional potential energy surface (PES). The main characteristics of the PES depend on the repulsive Coulomb potential and the attractive nuclear potential. The structural effects of the nuclei taking part in the reactions also play a certain role in shaping these surfaces. These modulations play a crucial role in deciding the final outcomes in reactions using heavy nuclei. The contact configuration of the nuclei in the PES (which is strongly influenced by the beam energy, static deformation of the reaction partners, and their relative orientations) is also very important in deciding the final observables in the reaction.

Most of these aspects were taken into consideration while calculating the capture probabilities in this work. While the possibility of interactions with different orientation angles are considered [47,48] for the deformed nuclei, surface vibrations have been taken into account for the spherical nuclei. Final results are averaged over all possible orientation angles (α_1 and α_2) of the axial symmetry axis of the deformed nuclei relative to the beam direction or the vibrational states of the spherical nuclei [49]. The deformation parameters used in the calculations are shown later in Table II.

The capture probability is significantly affected by the beam energy, orbital angular momentum, contact configuration in the PES, depth of the potential pocket, dissipative forces, and the dynamical nature of fusion process. In heavy systems, the DNS formed after capture need not always evolve towards the CN. The features in the PES may guide the DNS to breakup as quasifission products before achieving the compact

configuration of the CN. Thus, for a given $E_{\rm c.m.}$ and angular momentum ℓ, capture cross section $\sigma_{\rm cap}$ is the sum of fusion $\sigma_{\rm fus}$ and quasifission $\sigma_{\rm qfis}$ cross sections.

That is,

$$\sigma_{\rm cap}(E_{\rm c.m.},\ell;\alpha_1,\alpha_2) = \sigma_{\rm fus}(E_{\rm c.m.},\ell;\alpha_1,\alpha_2) + \sigma_{\rm qfis}(E_{\rm c.m.},\ell;\alpha_1,\alpha_2).$$

$\sigma_{\rm cap}$ is calculated using the equation

$$\sigma_{\rm cap}(E_{\rm c.m.},\ell;\alpha_1,\alpha_2) = \frac{\lambda^2}{4\pi}\sum_{\ell=0}^{\ell_d}(2\ell+1)P_{\rm cap}^{\ell}(E_{\rm c.m.},\ell;\alpha_1,\alpha_2),$$

where λ is the de Broglie wavelength associated with the entrance channel and ℓ_d is the maximal value of orbital angular momentum at which capture occurs for a given $E_{\rm c.m.}$. $P_{\rm cap}^{\ell}(E_{\rm c.m.},\ell;\alpha_1,\alpha_2)$ is the capture probability. ℓ_d is calculated by solving the equations of radial and tangential motion of the DNS [47,50]. $P_{\rm cap}^{\ell}(E_{\rm c.m.},\ell;\alpha_1,\alpha_2)$ is assumed to be unity if ℓ falls within the angular momentum window defined by $\ell_{\rm min}$ and ℓ_d, where $\ell_{\rm min}$ is the minimum orbital angular momentum leading to capture. $\ell_{\rm min} = 0$ for the reactions considered in this work. All other ℓ values falling outside this window do not contribute to capture.

The PES is calculated from the reaction energy balance (Q_{gg}) and the nucleus-nucleus potential (V) as [47,49]

$$U(Z_1,A_1,\ell,R,\{\alpha_i\}) = Q_{gg} + V(Z_1,A_1,\ell,R,\{\alpha_i\}), \quad (2)$$

where Z_1 and A_1 are the charge and mass numbers of a fragment of the DNS and R is the intercenter distance between its fragments (obviously for the other fragment, $Z_2 = Z_{\rm tot} - Z_1$, $A_2 = A_{\rm tot} - A_1$).

Q_{gg} is calculated from the binding energies of the interacting nuclei and the CN as

$$Q_{gg} = B_1 + B_2 - B_{\rm CN}, \quad (3)$$

where B_1, B_2, and $B_{\rm CN}$ are the binding energies of the DNS fragments and the CN, respectively, which are obtained from Ref. [51] if experimental data are available. Calculated values from Ref. [52] were taken otherwise.

B. CN formation

The DNS formed after a successful capture follow different trajectories in the PES during its evolution. The fusion and quasifission cross sections are calculated using the equations

$$\sigma_{\rm fus} = \sum_{\ell=0}^{\ell_d(E)}(2\ell+1)\sigma_{\rm cap}(E,\ell)P_{\rm CN}(E,\ell), \quad (4)$$

$$\sigma_{\rm qfis} = \sum_{\ell=0}^{\ell_d(E)}(2\ell+1)\sigma_{\rm cap}(E,\ell)[1-P_{\rm CN}(E,\ell)], \quad (5)$$

where $P_{\rm CN}$ is the fusion probability of the DNS. $P_{\rm CN}$ is calculated using the expression [47]

$$P_{\rm CN}(E^*_{\rm DNS},\ell;\alpha_i) = \sum_{Z_{\rm sym}}^{Z_{\rm max}} Y_Z(E^*_{\rm DNS})P^Z_{\rm CN}(E^*_{\rm DNS},\ell;\alpha_i). \quad (6)$$

Here $Z_{\rm sym}$ is the charge symmetry and $Z_{\rm max}$ correspond to the value of Z at which driving potential is the maximum. The value of $Z_{\rm max}$ depends on the orientation angles α_i ($i = 1,2$) of the DNS fragments [47] and orbital angular momentum ℓ [50]. $E^*_{\rm DNS}$ is the excitation energy of the DNS for a given value of charge configuration $(Z, Z_{\rm tot} - Z)$ where $Z_{\rm tot} = Z_P + Z_T$. Z_P and Z_T are the atomic numbers of the projectile and target, respectively. $Y_Z(E^*_{\rm DNS})$ is the probability of population of the DNS in such a configuration with $(Z, Z_{\rm tot} - Z)$ at $E^*_{\rm DNS}$, ℓ and given orientation α_i calculated following the method presented in Ref. [47].

The average values of capture and fusion cross sections were obtained by averaging the collisions of different orientation angles α_i. Deformation parameters of the ground quadrupole and octupole states are taken from Ref. [52], while those of the first excited 2^+ and 3^- states are obtained from Refs. [53,54], respectively. Nuclei which are spherical in shape in their ground state are treated as vibrating nuclei in this work, where the surface vibrations are treated as independent harmonic vibrations and the nuclear radius for such nuclei is considered to be distributed as a Gaussian form [49]. The deformation parameters of the ground state and the first excited 2^+ and 3^- states of different nuclei considered in this work are given in Table II.

C. ER cross sections

The ER cross sections were calculated using the statistical model [46] with the fusion angular momentum distributions generated from the DNS model as the input. The CN formed in a reaction decays rapidly by evaporating light particles (neutrons, protons, α particles), γ quanta, and fission. The total ER cross section at an intermediate excitation energy E^*_x is given by

$$\sigma^x_{\rm ER}(E^*_x) = \sum_{\ell=0}^{\ell_d}(2\ell+1)\sigma^x_{\rm ER}(E^*_x,\ell) \quad (7)$$

where $\sigma^x_{\rm ER}(E^*_x,\ell)$ is the partial cross section of ER formation obtained after all the energetically possible de-excitations such as neutron, proton, α particle, and γ emissions of the intermediate nucleus, with excitation energy E^*_x at each step x of de-excitation cascade [46,55]. The survival probability of the intermediate nucleus against fission $W^x_{\rm sur}$ is also considered in each step of the decay cascade. Thus,

$$\sigma^x_{\rm ER}(E^*_x,\ell) = \sigma^{x-1}_{\rm ER}(E^*_{x-1},\ell)W^x_{\rm sur}(E^*_x,\ell) \quad (8)$$

with the CN as the starting point. The overall survival probability $W_{\rm sur}(E^*_{\rm CN})$ excitation function versus $E^*_{\rm CN}$ of the CN is obtained as the ratio $W_{\rm sur}(E^*_{\rm CN}) = \sigma_{\rm ERtot}(E^*_{\rm CN})/\sigma_{\rm fus}(E^*_{\rm CN})$, where $\sigma_{\rm ERtot}(E^*_{\rm CN})$ is the sum of all partial cross sections of the ERs formed in all steps of the de-excitation cascade of the CN.

The fission barrier used in this work is the sum of a macroscopic component $B^m_{\rm fis}$ [56] and microscopic correction δW due to shell effects. The shell effects wash out with increasing beam energy. The damping of shell effects with increase in excitation energy and angular momentum were

included in the fission barrier height as [46]

$$B_{\rm fis}(\ell,T) = cB^m_{\rm fis} - h(T)q(\ell)\delta W, \quad (9)$$

where

$$h(T) = \{1+\exp[(T-T_0)/d]\}^{-1}$$

and

$$q(\ell) = \{1+\exp[(\ell-\ell_{1/2})/\Delta\ell]\}^{-1}$$

are the damping functions and $c = 1$. Here, T is the nuclear temperature given by $T = \sqrt{E^*/a}$, where E^* is the excitation energy. d is the rate at which shell effects wash out with excitation energy and $T_{\frac{1}{2}}$ is the temperature at which $h(T)$ is reduced by half. Similarly $\Delta\ell$ and $\ell_{\frac{1}{2}}$ represent the rate of washing out of shell corrections with angular momentum and value of ℓ at which $q(\ell)$ is reduced by 1/2, respectively. We used $d = 0.2$ MeV, $T_{\frac{1}{2}} = 1.15$ MeV, $\Delta\ell = 3\hbar$, and $\ell_{\frac{1}{2}} = 20\hbar$ in this work for all reactions considered.

For the determination of the collective level density parameter, which describes the total collective level density in the nonadiabatic approach, we take into account the intrinsic excitations and rotational and vibrational enhancement factors due to the coupling of the collective and intrinsic degrees of freedom. These enhancement factors are damped with excitation energy (E^*). We use the following expressions for the level density parameter (a) in this work:

$$a_n(E^*) = \tilde{a}\left\{1+\delta W\left[\frac{1-\exp(-\gamma E^*)}{E^*}\right]\right\}, \quad (10)$$

where $\tilde{a} = 0.094A$ is the asymptotic value and A is the mass number. γ (=0.064 MeV^{-1}) is the parameter which accounts for the rate at which shell effects wash out with excitation energy [57–59] for the neutron channel. For the fission channel, we used $a_f(E^*) = a_n(E^*) \times r(E^*)$, where $r(E^*) = \frac{\exp(\gamma_f E^*)-(1+E^*/\delta W)}{\exp(-\gamma E^*)-(1+E^*/\delta W)}$, with $\gamma_f(E^*) = 0.024$ MeV^{-1}.

VI. THEORETICAL RESULTS AND DISCUSSION

In this section, the experimental results are compared with the theoretical calculations. Calculations have also been performed for the ^{16}O + ^{194}Pt reaction (which was experimentally demonstrated to proceed through the CN formation) as a benchmark to understand the role of entrance channels in fusion. In addition to this, calculations have been extended to the ^{50}Ti + ^{160}Gd [60] reaction for which cross sections for some of the neutron evaporation channels are available. The reactions forming same CN through different entrance channels provide a systematic understanding of fusion and quasifission competition with increasing Coulomb factor in the reaction. The reactions forming the same CN, ^{210}Rn, are discussed first followed by the ^{28}Si + ^{180}Hf reaction forming the CN, ^{208}Rn.

A. ^{16}O + ^{194}Pt reaction

Among the three different entrance channels forming the nucleus of ^{210}Rn considered in this work, ^{16}O + ^{194}Pt is the most asymmetric reaction. ER [28] and fission fragment [21,61] measurements for this reaction clearly demonstrated that this reaction proceeds through the formation of the CN and ruled out the presence of quasifission. In Fig. 4, we compare the calculated fusion and total ER excitation functions with the experimental values for this reaction. The excitation functions of individual neutron evaporation channels ($3n$, $4n$, $5n$, and $6n$), sum of all possible neutron emission channels, and the capture excitation function are also shown in the same figure.

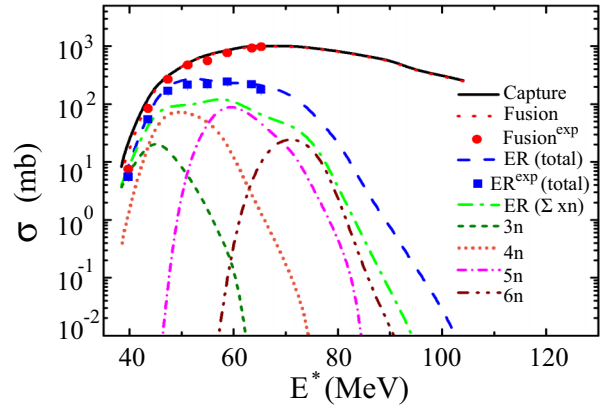

FIG. 4. Experimental total ER [28] and fusion excitation functions for the ^{16}O + ^{194}Pt reaction. Theoretical calculations for different neutron evaporation channels, sum of neutron evaporation channels, total ER, fusion, and capture cross sections are also shown.

It may be noticed that the calculations reproduce the experimental fusion and total ER excitation functions quite well at all energies measured. The fact that the calculated $\sigma_{\rm cap} = \sigma_{\rm fus}$ for $E^* = 40$–100 MeV emphasize the absence of non-compoundnuclear processes in this reaction. This may also be observed from the $P_{\rm CN}$ values for this reaction (solid black line) shown in Fig. 5. $P_{\rm CN}$ values are observed to be close to 1 in the entire range of excitation energy, indicating that the DNS formed in this reaction evolves completely towards the CN configuration after the capture.

B. ^{30}Si + ^{180}Hf reaction

Fission fragment mass distribution studies for the ^{30}Si + ^{180}Hf reaction reported earlier [21] indicated the onset

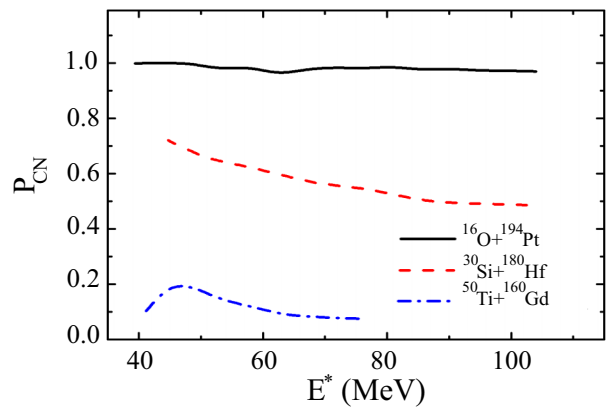

FIG. 5. Calculated values of fusion probability ($P_{\rm CN}$) for different reactions forming the CN ^{210}Rn.

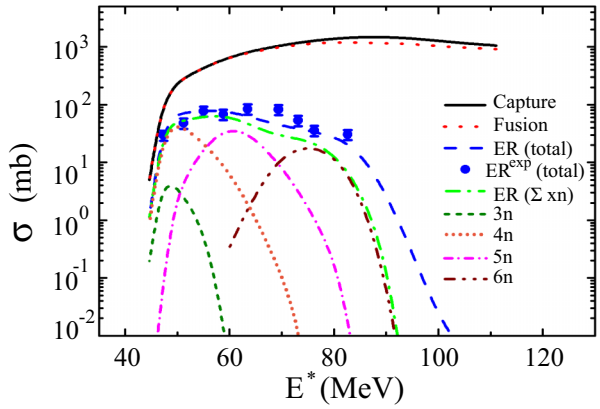

FIG. 6. Experimental total ER excitation function for the ^{30}Si + ^{180}Hf reaction compared with the theoretical calculations. The results for different neutron evaporation channels, sum of neutron channels, fusion, and capture cross sections are also shown.

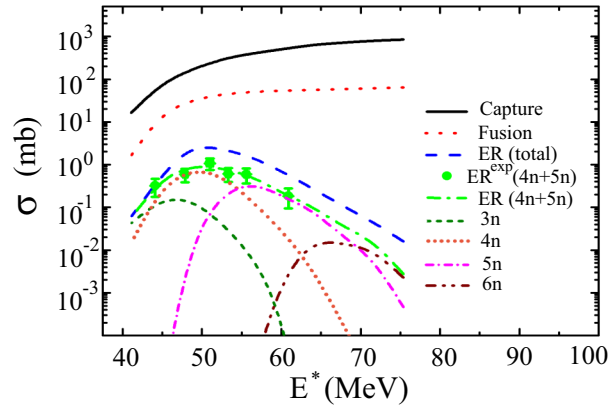

FIG. 7. Experimental ER cross sections for $4n + 5n$ channels [60] for the ^{50}Ti + ^{160}Gd reaction compared with the model calculations. The results for different neutron evaporation channels, sum of neutron channels, fusion, and capture cross sections are also shown.

of quasifission in this reaction. The calculated excitation functions for the capture, fusion, total ER, different neutron channels, and sum of all neutron channels are shown in Fig. 6, along with the total experimental ER excitation function. The experimental total ER cross sections are well reproduced by the model calculations. The calculated fusion cross sections are observed to be lower than the capture cross sections for this reaction, confirming the presence of quasifission, in consensus with the experimental findings.

The escape of DNS flux after capture, away from the CN configuration, is readily visible in the calculated $P_{\rm CN}$ values (red dashed line) for this reaction shown in Fig. 5. Unlike the ^{16}O + ^{194}Pt reaction, $P_{\rm CN}$ values are lower than 1 for this reaction at all energies. $P_{\rm CN}$ also shows a decreasing trend with increasing excitation energy. This could be due to the effect of angular momentum of the DNS formed in this reaction. The angular momentum of the DNS increases with increasing beam energy. It has been shown that the increase in angular momentum increases the intrinsic fusion barrier [49], which decreases the probability of CN formation.

The higher Coulomb factor ($Z_P Z_T = 1008$ for the ^{30}Si + ^{180}Hf and 624 for the ^{16}O + ^{194}Pt reactions, respectively) should be playing a crucial role in diverting part of the DNS flux at the capture stage to the quasifission channel during the evolution of the system. The larger deformation of the ^{180}Hf target may also be favoring this effect as the contact configuration in collisions with the deformed nuclei will be relatively away from the more compact configuration that would result from collisions with less deformed or spherical target nuclei.

C. ^{50}Ti + ^{160}Gd reaction

Recently, Mayorov *et al.* [60] measured the ER excitation function for the $4n + 5n$ channels for the ^{50}Ti + ^{160}Gd reaction, forming the same CN, ^{210}Rn. From a statistical model analysis, the authors reported a larger fission probability for this reaction than the predictions of Bohr-Wheeler theory and the observations were attributed to the influence of collective nuclear excitations. Even though the total ER cross section is not available for this reaction for a direct comparison of the experimental results, we included this reaction in our study as it serves the role of a much more symmetric reaction forming the same CN. Calculated capture, fusion, total ER, $\sum$xn, and $4n + 5n$ cross sections are shown in Fig. 7 along with the measured $4n + 5n$ cross sections. The model calculations are in good agreement with the available experimental results.

The very low $P_{\rm CN}$ values obtained for this reaction (blue dot-dashed line, Fig. 5) clearly point out that only a small fraction of the total capture flux successfully evolve towards CN in this reaction. Even though the calculations are constrained only by the $(4n + 5n)$ ER cross sections at the moment, the results are consistent with fission measurements reported for the Ti+Gd reaction. A strong mass-angle correlation [62] and wider mass distributions [63] have been reported for the ^{48}Ti + ^{162}Gd reaction, underlining the strong presence of quasifission in this reaction. Similar results are expected for the ^{50}Ti + ^{160}Gd reaction as indicated by the $P_{\rm CN}$ values (blue dot-dashed line) presented in Fig. 5.

D. ^{28}Si + ^{180}Hf reaction

Unlike the three reactions discussed before, the ^{28}Si + ^{180}Hf reaction populates the CN ^{208}Rn in the fusion process. The results of model calculation and experiment are shown in Fig. 8. The measured cross section is observed to be much higher than the model estimate at $E^* = 106.0$ MeV for this reaction. The calculations instead predict a steep decrease of total ER cross section at such high excitation energies. Any possible uncertainty that is originating from the linear extrapolation method used for estimating the transmission efficiency and thus the cross section at this energy cannot explain the two orders of magnitude difference observed in the experimental and calculated cross-section numbers.

A comprehensive analysis of the high-energy data where the experimental results deviate significantly from the model calculations is out of the scope of this paper, primarily due to

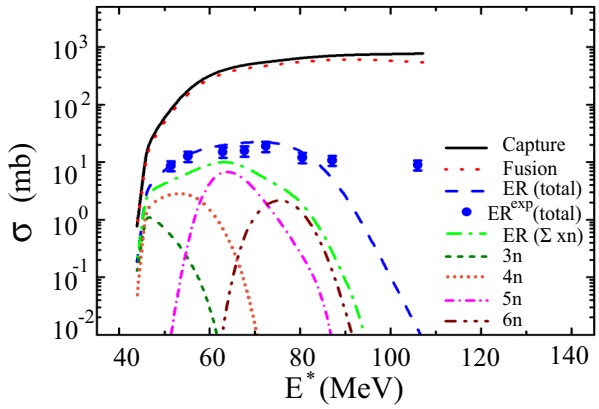

FIG. 8. Same as Fig. 6, but for the ^{28}Si + ^{180}Hf reaction.

the lack of data points between 87.1 and 106.0 MeV. Below 87.1 MeV, the experimental results are in good agreement with the theoretical calculations. A calculation assuming the evolution and decay of a DNS formed from the projectile after an α particle emission yields a cross section of about 7 mb, reasonably close to the measured cross section of 8.97 mb. It has been reported [64,65] that such projectile breakup processes might stem from the high angular momentum collisions and compete principally with fission. The dissipative effects associated with higher angular momentum collisions could be another possibility, as dissipative forces delay fission and favor particle evaporation [66–70], leading to larger ER cross sections. In any case, this observation at the high-energy cross section calls for more ER measurements at very high excitation energies in heavy-ion fusion reactions.

E. General remarks

Except for the ^{16}O + ^{194}Pt reaction, all other reactions studied in this paper show significant component of quasi-fission in the total capture cross sections. The rapid fall of fusion probability with increase in charge product ($Z_P Z_T$) in the reactions forming ^{210}Rn CN clearly demonstrate the strong influence of entrance channels in deciding the capture outcomes. This is reflected as the reduction in ER cross section in the more symmetric systems compared with the ^{16}O + ^{194}Pt reaction at similar CN excitation energies.

A comparison of the relative ER yields from the two reactions ^{28,30}Si + ^{180}Hf measured in this work (as can be seen from Fig. 2) show larger ER cross sections for the ^{30}Si induced reaction populating the heavier isotope of radon. In order to understand this observation, we studied the ER cross sections of different radon compound systems populated using beams of Si (^{28,29,30}Si) on Hf (^{178,180}Hf) targets. In Fig. 9(a), we compare the measured ER cross sections for different reactions populating different isotopes of radon as CN. Cross-section data for the ^{28,29}Si + ^{178}Hf reactions were taken from Refs. [23,24]. An increase of ER cross section with increasing mass in the isotopic chain of the CN may be observed from the comparison made in Fig. 9(a). Similar observations may be made from other reactions reported in literature [71–73].

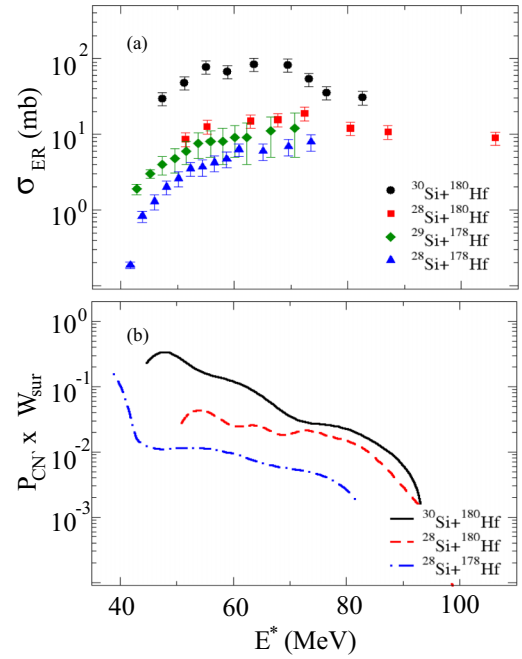

FIG. 9. (a) Total ER cross section for different Si+Hf reactions populating isotopes of radon as CN, as a function of excitation energy. (b) ER formation probability ($P_{CN} \times W_{sur}$) for different reactions populating ^{206,208,210}Rn.

In heavy nuclei, the ER formation probability is decided by the two competing processes—first the quasifission and later the fusion-fission. Once the CN is formed, the fission barrier height, excitation energy, and the angular momentum populated play crucial roles in deciding the decay of the CN. One possible reason for the larger ER cross sections observed in heavier isotopes of the CN could be the reduced fissility of such nuclei with increase in neutron number. The neutron binding energy decreases with increase in neutron number, which also favors neutron evaporation in heavy CN. Considering the hurdles faced by the fusing system from the entrance channel configuration to the ER formation stage, the product of P_{CN} and W_{sur} as a function of E^* should consistently represent the experimental observables. This product is shown in Fig. 9(b) for the two reactions measured in this work and the reaction ^{28}Si + ^{178}Hf that populates the lightest CN shown in Fig. 9(a). The trend of $P_{CN} \times W_{sur}$ unambiguously explain the experimental observations made for different isotopes of Rn formed in fusion reactions.

VII. SUMMARY AND CONCLUSIONS

ER cross sections have been measured for the ^{28,30}Si + ^{180}Hf reactions forming the compound systems ^{208}Rn and ^{210}Rn, respectively. Larger ER cross sections have been observed with increase in mass in the isotopic chain of the CN. This could be explained by considering the fusion and survival probabilities of the compound system formed. Increase of neutron number (and hence the mass number) decreases the neutron binding energy and the fissility of the CN, both favoring the neutron evaporation over fission decay in heavy isotopes.

A comparison of the ER cross sections for the reactions populating the same CN at similar excitation energies clearly demonstrates a reduction in ER cross sections for more symmetric reactions with larger $Z_P Z_T$ values. This reduction is a direct signature of fusion hindrance due to quasifission process in heavier systems and its dependence on entrance channels. Experimental observations are consistent with the fission fragment mass [21] and angular distributions [40] studies in this mass region.

The effects of entrance channels on the capture, fusion, and ER formation probabilities are studied by comparing the experimental results with the calculations using combined dinuclear and advanced statistical models. Calculations are in complete agreement with the experimental observations for the most asymmetric reaction (^{16}O + ^{194}Pt) considered, yielding complete fusion in the entire range of energies over which experimental data are available. The fusion probability drops to 60–70% for the ^{30}Si + ^{180}Hf reaction and less than 20% for the ^{50}Ti + ^{160}Gd reaction, reflecting the strong effect of Coulomb factor in shaping the PES to decide the final outcome of the reaction. Quasifission is also observed in the total capture cross sections for the ^{28}Si + ^{180}Hf reaction, consistent with the recent results of fission angular distribution studies in this reaction.

An observation for the ^{28}Si + ^{180}Hf reaction is the unexpectedly large ER cross section measured at $E^* = 106$ MeV, differing significantly from the model calculations. A calculation assuming incomplete fusion of the projectile may reproduce the cross section at such high excitations. However, the absence of intermediate data points limits a detailed theoretical exploration at the moment, calling for more measurements at such high excitation energies.

ACKNOWLEDGMENTS

The authors are grateful to the Pelletron and Linac accelerator staff of the IUAC for their excellent support during the experiments. One of the authors (A.S.) acknowledges support from the University Grants Commission (UGC), India, in the form of a MANF fellowship to carry out this work. M.S. Acknowledges support from the Kerala State Council for Science, Technology and Environment (KSCSTE) in the form of a fellowship. E.P. acknowledges Dr. S. Pal for illuminating discussions.

[1] S. Hofmann and G. Münzenberg, Rev. Mod. Phys. **72**, 733 (2000).
[2] J. H. Hamilton, S. Hofmann, and Y. T. Oganessian, Annu. Rev. Nucl. Part. Sci. **63**, 383 (2013).
[3] Y. T. Oganessian and V. K. Utyonkov, Rep. Prog. Phys. **78**, 036301 (2015).
[4] W. J. Swiatecki, Phys. Scr. **24**, 113 (1981).
[5] S. Bjørnholm and W. J. Swiatecki, Nucl. Phys. A **391**, 471 (1982).
[6] J. Tōke *et al.*, Nucl. Phys. A **440**, 327 (1985).
[7] J. P. Blocki, H. Feldmeier, and W. J. Swiatecki, Nucl. Phys. A **459**, 145 (1986).
[8] A. C. Berriman, D. J. Hinde, M. Dasgupta, C. R. Morton, R. D. Butt, and J. O. Newton, Nature (London) **413**, 144 (2001).
[9] C.-C. Sahm, H.-G. Clerc, K.-H. Schmidt, W. Reisdorf, P. Armbruster, F. P. Heßberger, J. G. Keller, G. Münzenberg, and D. Vermeulen, Z. Phys. A **319**, 113 (1984).
[10] D. J. Hinde and M. Dasgupta, Phys. Lett. B **622**, 23 (2005).
[11] K. Nishio, S. Mitsuoka, I. Nishinaka, H. Makii, Y. Wakabayashi, H. Ikezoe, K. Hirose, T. Ohtsuki, Y. Aritomo, and S. Hofmann, Phys. Rev. C **86**, 034608 (2012).
[12] K. Nishio, H. Ikezoe, S. Mitsuoka, I. Nishinaka, Y. Nagame, Y. Watanabe, T. Ohtsuki, K. Hirose, and S. Hofmann, Phys. Rev. C **77**, 064607 (2008).
[13] D. J. Hinde, R. du Rietz, M. Dasgupta, R. G. Thomas, and L. R. Gasques, Phys. Rev. Lett. **101**, 092701 (2008).
[14] D. J. Hinde, M. Dasgupta, J. R. Leigh, J. C. Mein, C. R. Morton, J. O. Newton, and H. Timmers, Phys. Rev. C **53**, 1290 (1996).
[15] D. J. Hinde, R. G. Thomas, R. du Rietz, A. Diaz-Torres, M. Dasgupta, M. L. Brown, M. Evers, L. R. Gasques, R. Rafiei, and M. D. Rodriguez, Phys. Rev. Lett. **100**, 202701 (2008).
[16] D. J. Hinde, M. Dasgupta, J. R. Leigh, J. P. Lestone, J. C. Mein, C. R. Morton, J. O. Newton, and H. Timmers, Phys. Rev. Lett. **74**, 1295 (1995).
[17] G. N. Knyazheva, E. M. Kozulin, R. N. Sagaidak, A. Y. Chizhov, M. G. Itkis, N. A. Kondratiev, V. M. Voskressensky, A. M. Stefanini, B. R. Behera, L. Corradi, E. Fioretto, A. Gadea, A. Latina, S. Szilner, M. Trotta, S. Beghini, G. Montagnoli, F. Scarlassara, F. Haas, N. Rowley, P. R. S. Gomes, and A. Szantode Toledo, Phys. Rev. C **75**, 064602 (2007).
[18] C. Simenel, D. J. Hinde, R. du Rietz, M. Dasgupta, M. Evers, C. J. Lin, D. H. Luong, and A. Wakhle, Phys. Lett. B **710**, 607 (2012).
[19] A. Wakhle, C. Simenel, D. J. Hinde, M. Dasgupta, M. Evers, D. H. Luong, R. du Rietz, and E. Williams, Phys. Rev. Lett. **113**, 182502 (2014).
[20] E. Prasad, K. M. Varier, R. G. Thomas, P. Sugathan, A. Jhingan, N. Madhavan, B. R. S. Babu, R. Sandal, S. Kalkal, S. Appannababu, J. Gehlot, K. S. Golda, S. Nath, A. M. Vinodkumar, B. P. AjithKumar, B. V. John, G. Mohanto, M. M. Musthafa, R. Singh, A. K. Sinha, and S. Kailas, Phys. Rev. C **81**, 054608 (2010).
[21] A. Shamlath *et al.*, Nucl. Phys. A **945**, 67 (2016).
[22] T. Banerjee, S. Nath, and S. Pal, Phys. Rev. C **91**, 034619 (2015).
[23] R. D. Butt, D. J. Hinde, M. Dasgupta, A. C. Berriman, A. Mukherjee, C. R. Morton, and J. O. Newton, Phys. Rev. C **66**, 044601 (2002).
[24] R. D. Butt, Ph.D. thesis, Australian National University, Canberra, Australia, 2013 (unpublished).
[25] P. N. Prakash *et al.*, Pramana **59**, 849 (2002).
[26] S. Ghosh, R. Mehta, G. K. Chowdhury, A. Rai, P. Patra, B. K. Sahu, A. Pandey, D. S. Mathuria, J. Chacko, A. Chowdhury, S. Kar, S. Babu, M. Kumar, S. S. K. Sonti, K. K. Mistry, J. Zacharias, P. N. Prakash, T. S. Datta, A. Mandal, D. Kanjilal, and A. Roy, Phys. Rev. ST Accel. Beams **12**, 040101 (2009).
[27] N. Madhavan *et al.*, Pramana **75**, 317 (2010).
[28] E. Prasad, K. M. Varier, N. Madhavan, S. Nath, J. Gehlot, S. Kalkal, J. Sadhukhan, G. Mohanto, P. Sugathan, A. Jhingan,

B. R. S. Babu, T. Varughese, K. S. Golda, B. P. Ajith Kumar, B. Satheesh, S. Pal, R. Singh, A. K. Sinha, and S. Kailas, Phys. Rev. C **84**, 064606 (2011).
[29] S. Nath, A Monte Carlo code to model ion transport in dilute gas medium (unpublished).
[30] A. Jinghan, Pramana **85**, 483 (2015).
[31] S. Nath, P. V. Rao, S. Pal, J. Gehlot, E. Prasad, G. Mohanto, S. Kalkal, J. Sadhukhan, P. D. Shidling, K. S. Golda, A. Jhingan, N. Madhavan, S. Muralithar, and A. K. Sinha, Phys. Rev. C **81**, 064601 (2010).
[32] B. B. Back *et al.*, Nucl. Instrum. Methods Phys. Res., Sect. A **379**, 206 (1996).
[33] A. M. Vinodkumar, K. M. Varier, N. V. S. V. Prasad, D. L. Sastry, A. K. Sinha, N. Madhavan, P. Sugathan, D. O. Kataria, and J. J. Das, Phys. Rev. C **53**, 803 (1996).
[34] D. J. Hinde, A. C. Berriman, R. D. Butt, M. Dasgupta, I. I. Gontchar, C. R. Morton, A. Mukherjee, and J. O. Newton, J. Nucl. Radiochem. Sci. **3**, 31 (2002).
[35] R. A. Broglia and A. Winther, *Heavy Ion Reaction Lecture Notes, Vol. 1: Elastic and Inelastic Reactions* (Benjamin/Cummings, Reading, MA, 1981).
[36] K. Hagino, N. Rowley, and A. T. Kruppa, Comput. Phys. Commun. **123**, 143 (1999).
[37] B. B. Back, R. R. Betts, J. E. Gindler, B. D. Wilkins, S. Saini, M. B. Tsang, C. K. Gelbke, W. G. Lynch, M. A. McMahan, and P. A. Baisden, Phys. Rev. C **32**, 195 (1985).
[38] W. Q. Shen, J. Albinski, A. Gobbi, S. Gralla, K. D. Hildenbrand, N. Herrmann, J. Kuzminski, W. F. J. Muller, H. Stelzer, J. Toke, B. B. Back, S. Bjornholm, and S. P. Sorensen, Phys. Rev. C **36**, 115 (1987).
[39] R. Vandenbosch and J. R. Huizenga, *Nuclear Fission* (Academic Press, New York, 1973).
[40] T. Banerjee *et al.*, Phys. Rev. C **94**, 044607 (2016).
[41] D. J. Hinde, M. Dasgupta, and A. Mukherjee, Phys. Rev. Lett. **89**, 282701 (2002).
[42] V. I. Zagrebaev and W. Greiner, Phys. Rev. C **78**, 034610 (2008).
[43] W. J. Swiatecki, K. Siwek-Wilczynska, and J. Wilczynski, Phys. Rev. C **71**, 014602 (2005).
[44] K. Siwek-Wilczyńska, A. Borowiec, I. Skwira-Chalot, and J. Wilczyński, Int. J. Mod. Phys. E **17**, 12 (2008).
[45] R. Yanez, W. Loveland, J. S. Barrett, L. Yao, B. B. Back, S. Zhu, and T. L. Khoo, Phys. Rev. C **88**, 014606 (2013).
[46] G. Mandaglio, G. Giardina, A. K. Nasirov, and A. Sobiczewski, Phys. Rev. C **86**, 064607 (2012).
[47] A. Nasirov, A. Fukushima, Y. Toyoshima, Y. Aritomo, A. Muminov, S. Kalandarov, and R. Utamuratov, Nucl. Phys. A **759**, 342 (2005).
[48] G. Fazio, G. Giardina, F. Hanappe, G. Mandaglio, M. Manganaro, A. I. Muminov, A. K. Nasirov, and C. Saccá, J. Phys. Soc. Jpn. **77**, 124201 (2008).
[49] K. Kim, Y. Kim, A. K. Nasirov, G. Mandaglio, and G. Giardina, Phys. Rev. C **91**, 064608 (2015).
[50] G. Fazio, G. Giardina, G. Mandaglio, R. Ruggeri, A. I. Muminov, A. K. Nasirov, Y. T. Oganessian, A. G. Popeko, R. N. Sagaidak, A. V. Yeremin, S. Hofmann, F. Hanappe, and C. Stodel, Phys. Rev. C **72**, 064614 (2005).
[51] G. Audi and A. H. Wapstra, Nucl. Phys. A **595**, 409 (1995).
[52] P. Möller, J. R. Nix, W. D. Myers, and W. J. Swiatecki, At. Data Nucl. Data Tables **59**, 185 (1995).
[53] S. Raman, C. W. Nestor Jr., and P. Tikkanen, At. Data Nucl. Data Tables **78**, 1 (2001).
[54] R. H. Spear, At. Data Nucl. Data Tables **42**, 55 (1989).
[55] G. Giardina, S. Hofmann, A. I. Muminov, and A. K. Nasirov, Eur. Phys. J. A **8**, 205 (2000).
[56] A. J. Sierk, Phys. Rev. C **33**, 2039 (1986).
[57] A. V. Ignatyuk, G. N. Smirenkin, and A. S. Tishin, Sov. J. Nucl. Phys. **21**, 255 (1975).
[58] A. D'Arrigo, G. Giardina, M. Herman, A. V. Ignatyuk, and A. Taccone, J. Phys. G: Nucl. Part. Phys. **20**, 365 (1994).
[59] A. D'Arrigo, G. Giardina, M. Herman, and A. Taccone, Phys. Rev C **46**, 1437 (1992).
[60] D. A. Mayorov, T. A. Werke, M. C. Alfonso, E. E. Tereshatov, M. E. Bennett, M. M. Frey, and C. M. Folden III, Phys. Rev. C **92**, 054601 (2015).
[61] E. Prasad *et al.*, Nucl. Phys. A **882**, 62 (2012).
[62] R. du Rietz, E. Williams, D. J. Hinde, M. Dasgupta, M. Evers, C. J. Lin, D. H. Luong, C. Simenel, and A. Wakhle, Phys. Rev. C **88**, 054618 (2013).
[63] C. J. Lin, R. du Rietz, D. J. Hinde, M. Dasgupta, R. G. Thomas, M. L. Brown, M. Evers, L. R. Gasques, and M. D. Rodriguez, Phys. Rev. C **85**, 014611 (2012).
[64] P. Vergani, E. Gadioli, E. Vaciago, E. Fabrici, E. Gadioli Erba, M. Galmarini, G. Ciavola, and C. Marchetta, Phys. Rev. C **48**, 1815 (1993).
[65] S. Chakrabarty, B. S. Tomar, A. Goswami, G. K. Gubbi, S. B. Manohar, A. Sharma, B. Bindukumar, and S. Mukerjee, Nucl. Phys. A **678**, 355 (2000).
[66] M. G. Itkis and A. Ya. Rusanov, Phys. Part. Nucl. **29**, 160 (1998).
[67] D. Hilscher and H. Rossner, Ann. Phys. Fr. **17**, 471 (1992).
[68] B. B. Back, D. J. Blumenthal, C. N. Davids, D. J. Henderson, R. Hermann, D. J. Hofman, C. L. Jiang, H. T. Penttila, and A. H. Wuosmaa, Phys. Rev. C **60**, 044602 (1992).
[69] P. D. Shidling, N. M. Badiger, S. Nath, R. Kumar, A. Jhingan, R. P. Singh, P. Sugathan, S. Muralithar, N. Madhavan, A. K. Sinha, S. Pal, S. Kailas, S. Verma, K. Kalita, S. Mandal, R. Singh, B. R. Behera, K. M. Varier, and M. C. Radhakrishna, Phys. Rev. C **74**, 064603 (2006).
[70] V. Singh *et al.*, Phys. Rev. C **87**, 064601 (2013).
[71] R. N. Sagaidak and A. N. Andreyev, Phys. Rev. C **79**, 054613 (2009).
[72] S. Mitsuoka, H. Ikezoe, K. Nishio, K. Satou, and J. Lu, Phys. Rev. C **65**, 054608 (2002).
[73] K. Satou, H. Ikezoe, S. Mitsuoka, K. Nishio, and S. C. Jeong, Phys. Rev. C **65**, 054602 (2002).